IJMMM International Journal of Minerals, Metallurgy and Materials 矿物冶金与材料学报（英文版）

Effects of CeO_2 pre-calcined at different temperatures on the performance of Pt/CeO_2–C electrocatalyst for methanol oxidation reaction

Guo-qing Li, Pu-kang Wen, Chen-qiang Gao, Tian-yi Zhang, Jun-yang Hu, Yu-hao Zhang, Shi-you Guan, Qing-feng Li, and Bing Li

Cite this article as:
Guo-qing Li, Pu-kang Wen, Chen-qiang Gao, Tian-yi Zhang, Jun-yang Hu, Yu-hao Zhang, Shi-you Guan, Qing-feng Li, and Bing Li, Effects of CeO_2 pre-calcined at different temperatures on the performance of Pt/CeO_2–C electrocatalyst for methanol oxidation reaction, *Int. J. Miner. Metall. Mater.*, 28(2021), No. 7, pp. 1224-1232. https://doi.org/10.1007/s12613-020-2076-2

View the article online at SpringerLink or IJMMM Webpage.

International Journal of Minerals, Metallurgy and Materials
Volume 28, Number 7, July 2021, Page 1224
https://doi.org/10.1007/s12613-020-2076-2

Effects of CeO_2 pre-calcined at different temperatures on the performance of Pt/CeO_2–C electrocatalyst for methanol oxidation reaction

Guo-qing Li[1),*], *Pu-kang Wen*[1),*], *Chen-qiang Gao*[2)], *Tian-yi Zhang*[2)], *Jun-yang Hu*[2)], *Yu-hao Zhang*[2)], *Shi-you Guan*[3)], *Qing-feng Li*[4)], *and Bing Li*[1)]

1) School of Mechanical and Power Engineering, East China University of Science and Technology, Shanghai 200237, China
2) School of Materials Science and Engineering, East China University of Science and Technology, Shanghai 200237, China
3) Institute for Sustainable Energy, College of Sciences, Shanghai University, Shanghai 200237, China
4) Department of Energy Conversion and Storage, Technical University of Denmark, Lyngby 2800, Denmark
(Received: 25 March 2020; revised: 19 April 2020; accepted: 21 April 2020)

Abstract: Pt/CeO_2–C catalysts with CeO_2 pre-calcined at 300–600°C were synthesized by combining hydrothermal calcination and wet impregnation. The effects of the pre-calcined CeO_2 on the performance of Pt/CeO_2–C catalysts in methanol oxidation were investigated. The Pt/CeO_2–C catalysts with pre-calcined CeO_2 at 300–600°C showed an average particle size of 2.6–2.9 nm and exhibited better methanol electro-oxidation catalytic activity than the commercial Pt/C catalyst. In specific, the Pt/CeO_2–C catalysts with pre-calcined CeO_2 at 400°C displayed the highest electrochemical surface area value of 68.14 $m^2 \cdot g^{-1}$ and I_f/I_b ratio (the ratio of the forward scanning peak current density (I_f) and the backward scanning peak current density (I_b)) of 1.26, which are considerably larger than those (53.23 $m^2 \cdot g^{-1}$ and 0.79, respectively) of the commercial Pt/C catalyst, implying greatly enhanced CO tolerance.

Keywords: direct methanol fuel cell; platinum/cerium dioxide–carbon; electrocatalyst; methanol oxidation

1. Introduction

Methanol is an abundant and environment-friendly resource, and direct methanol fuel cells (DMFCs) have been attracted extensive research because of their high volumetric energy density and suitability for portable applications [1]. Nevertheless, the extensive commercial applications of DMFCs are restrained by several barriers, such as heat and water management, methanol crossover through the polymer proton exchange membrane, the slow kinetic reaction of methanol, and the poor stability of catalysts [2]. In specific, the intermediate CO produced during the anodic process can heavily poison the surface of Pt catalysts and slow down the kinetic reaction of methanol. The most efficient method to overcome this problem is to utilize Pt-based alloys [3–4], such as Ru [5–9], Ni [10], Co [11], and Sn [12], which were chosen for their oxophilicity. The additional metals can easily adsorb oxygen species such as OH_{ad}, which can facilitate the transformation of CO to CO_2 through a known bi-functional mechanism [13]. However, such a multi-component metallic electrocatalyst system is hard to achieve uniform nanostructure, impractical for commercial utilization, and is prone to segregation during device operation [14].

Another effective strategy is to use metal oxides as Pt catalyst support, which can significantly enhance the activity and stability of catalysts [15]. Nowadays, many metal oxides, such as WO_3 [16], SnO_2 [17], TiO_2 [18–19], and MoO_3 [20–21], have attracted considerable attention. In particular, ceria (cerium oxide) is efficient for alleviating gaseous CO poisoning because its fluorite structure provides high surface area and variable valence states (redox Ce^{3+}/Ce^{4+} sites) that increase oxygen storage capacity [14]. Moreover, the interaction between CeO_2 and Pt can enhance electrochemical activity by promoting the dispersion of Pt nanoparticles and allow OH_{ad} species to interact with CO on the Pt surface. The boundaries between Pt and CeO_x are active sites for oxygen reduction reaction (ORR). Therefore, with the addition of CeO_2, the Pt/CeO_2 catalytic system can not only enhance the electrochemical activity of methanol oxidation reaction (MOR) but also alleviate CO poisoning [22].

*These authors contributed equally to this work.

Corresponding authors: Shi-you Guan E-mail: syguan@shu.edu.cn; Bing Li E-mail: drlibing@163.com, bingli@ecust.edu.cn

Some scholars have reported that the addition of ceria improves the performance of Pt catalysts in methanol oxidation. Yu *et al.* [23] found that Pt/CeO_2–graphene catalysts exhibit better methanol electrochemical oxidation than Pt/graphene catalysts. CeO_2 content also affects ORR catalysis. Xu *et al.* [24] reported that Pt/CeO_2/C has more oxygen atoms than the sample without CeO_2. In specific, the percentage of surface oxygen on Pt nano-particles (NPs) is increased from 59.65% in Pt/C to 69.19% in Pt/20CeO_2/C containing 20wt% CeO_2 and to 77.75% in Pt/40CeO_2/C containing 40wt% CeO_2. The extremely enhanced oxygen spillover from CeO_2 to Pt surface increases ORR activity. X-ray photoelectron spectrometry (XPS) revealed that the Ce 3d peaks of Pt/CeO_2/C show a slightly negative shift when compared with those of pristine CeO_2, which is a strong evidence of the interaction between Pt and Ce. However, a high CeO_2 content inevitably leads to a rather low Pt^0 proportion and heavy aggregation, which reduces the number of active sites available. The strong interaction between Pt and Ce can increase the number of oxygen atoms on the Pt surface, but the preparation method, the CeO_2 content, the ratio of Ce^{3+}, and many other conditions may change the structure of the Pt/CeO_x system, which in turn affects catalytic activity.

Although many studies have investigated the effects of CeO_2 composition on Pt/CeO_2–C catalysts [25–27], few studies have discussed the influence of CeO_2 pre-calcined temperatures on MOR performance. Pt/CeO_2–C catalysts with CeO_2 pre-calcined at 300–600°C were investigated by the combination of hydrothermal calcination [28] and wet impregnation [29] to explore the optimal pre-calcination temperature of CeO_2 in methanol electro-oxidation. The electrocatalytic activity and stability of the as-synthesized catalysts in MOR were characterized by cyclic voltammetry (CV) and amperometric current density–time (*i*–*t*) curve analysis. Electrochemical results of this study show that the Pt/CeO_2–C catalyst with CeO_2 pre-calcined at 400°C exhibited superior CO tolerance in methanol electrochemical oxidation than the commercial Pt/C catalyst.

2. Experimental

2.1. Preparation of Pt/CeO_2–C nanocatalysts

(1) Synthesis of CeO_2/C precursor.

For the synthesis of the CeO_2/C precursor, 0.051 g $Ce(NO_3)_3 \cdot 6H_2O$ and 0.1896 g carbon substrate (Vulcan XC-72R, Cabot, America) were dissolved in 40 mL distilled water, and then the mixture was ultrasonicated for 30 min, continuously stirred for another 3 h, and then added with 50wt% ammonia until the pH value of the solution was 10. After the reaction, the mixture was filtered for three to five times. The obtained material was dried at 80°C for 12 h. Then, the dried material was calcined in a saturated nitrogen atmosphere at different high temperatures (300, 400, 500, and 600°C) for 2 h to obtain a homogeneous precursor CeO_2/C.

(2) Synthesis of Pt/CeO_2–C catalyst.

The previously prepared CeO_2/C precursor was dispersed in distilled water with another 30 min of pre-ultrasonication. The mixture was dropped with 16.7 mL H_2PtCl_6 solution (19.3 mmol/L) with continuous stirring for 1 h, and then placed in the oven until completely dry. The final product Pt/CeO_2–C catalyst was obtained after the reduction under 5% H_2/Ar at 300°C for 2 h. The obtained Pt/CeO_2–C samples at different pre-calcination temperatures (300, 400, 500, and 600°C) for CeO_2 were marked as PC300, PC400, PC500, and PC600, respectively.

(3) Preparation of working electrode.

For the fabrication of the working electrode, 10 mg catalysts in 5 mL isopropanol and 100 μL Nafion (10wt%, DE1020, DuPont, America) solution (0.05wt% Nafion dissolved in isopropanol) were mixed and then ultrasonicated for 30 min to obtain a homogeneous catalyst ink. Then, 8–12 μL of the catalyst ink was added onto the glassy carbon substrate with a micropipette, yielding a Pt load of 20 $\mu g \cdot cm^{-2}$. The glass carbon working electrode was polished with 50 nm alumina powder and then ultrasonicated with ultrapure water and ethanol for several times before all electrochemical measurements.

2.2. Characterization of physical properties

The X-ray diffraction (XRD) patterns were obtained with a Rigaku D/max 2550/PC diffractometer (RIGAKU, Japan) operating with graphite-monochromatized Cu K_α radiation (λ = 0.154060 nm), and scans were performed at the 2θ range of 10°–80°. The microstructure of the catalysts was analyzed by JEM-2100 transmission electron microscopy (TEM; JEOL, Japan). Chemical composition was analyzed by inductively coupled plasma-atomic emission spectroscopy (ICP-AES; iCAP 6000 Radial, THERMO, Varian, America). The surface electron structure of Pt/CeO_2–C was analyzed by XPS with a Thermo ESCALab250 using monochromatized Al K_α radiation.

2.3. Electrochemical characterization

All measurements were carried out in a conventional three-electrode cell at room temperature with a CHI 660D electrochemical analyzer (Chen Hua Instruments, Shanghai, China). The glassy carbon coated with the catalyst ink served as the working electrode, a platinum foil of 1 cm^2 as the counter electrode, and a saturated calomel electrode as the reference electrode. All the potentials were converted to reversible hydrogen electrode (RHE) after the measurements.

CV tests were performed in a 0.5 M N_2-purged H_2SO_4 solution at room temperature. The potential was scanned in the range of 0–1.2 V vs. RHE at a scan rate of 50 $mV \cdot s^{-1}$ for 40 cycles. The electrochemical surface area (ECSA) of each catalyst was calculated on the basis of the charges associated

with the adsorption peak of hydrogen after double-layer correction at the positive scanning, and the calculation equation is as follows [30–32]:

$$\mathrm{ECSA} = \frac{Q_{\mathrm{H}}}{210 W_{\mathrm{Pt}}} \quad (1)$$

where Q_{H} is the total charge (μC) calculated by the hydrogen adsorption peak area, W_{Pt} is the loading (μC·cm^{-2}) of Pt on the working electrode, and the constant "210" represents the charge needed to oxidize a monolayer of hydrogen on a bright Pt surface.

3. Results and discussion

3.1. Structure and composition analysis

Fig. 1 shows the XRD patterns of the PC400 catalyst and the precursor CeO_2/C pre-calcined at different temperatures (300, 400, 500, and 600°C). First, the diffraction peaks at 2θ= 39.85°, 46.30°, and 67.50° can be clearly found in the PC400 sample, which can be indexed as the (111), (200), and (220) planes of the Pt face centered cubic (fcc) crystalline structure, respectively, whereas the diffraction peaks belonging to CeO_2 cannot be recognized in the PC400 sample. For the precursor patterns, the diffraction peaks at 28.21°, 32.92°, 47.24°, and 56.20° are ascribed to the (111), (200), (220), and (311) planes of the CeO_2 cubic fluorite structure [33–34], respectively. Interestingly, the peak intensity of these facets increased with increasing pre-calcination temperature. The disappeared CeO_2 diffraction peaks in the PC400 sample may be assigned to the stronger Pt diffraction peaks hiding the CeO_2 diffraction peaks. The amorphous cerium oxide layer on Pt can prevent the Pt surface from oxidation and consequently enhance the activity of the catalysts [35]. In addition, another diffraction peak can be observed at 25.3°, which belongs to the (002) plane of carbon.

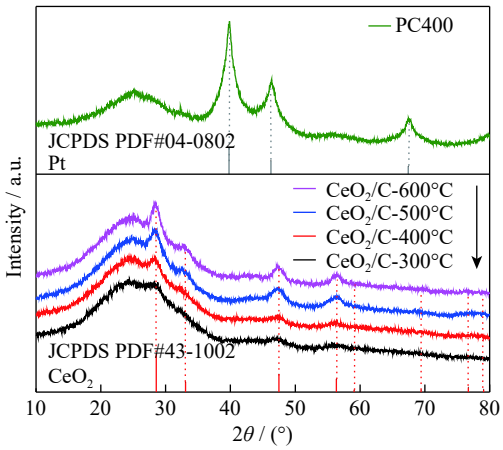

Fig. 1. XRD patterns of PC400 and CeO_2/C pre-calcined at different temperatures. Standard patterns of CeO_2 (JCPDS PDF#43-1002) and Pt (JCPDS PDF#04-0802) are attached for comparison.

Fig. 2 shows the TEM results of the as-synthesized Pt/CeO_2–C catalysts pre-calcined at different temperatures. In general, the four catalysts showed comparatively small sizes of about 2.7, 2.6, 2.7, and 2.9 nm. It should be noted that the red histograms represent the statistics of the number of particles in the corresponding TEM images, and the blue line represents the cumulative results of the proportion of different particle sizes. However, the high pre-calcination temperature (>400°C) led to the agglomeration of CeO_2 and the uneven distribution of Pt nanoparticles. An interplanar spacing distance of 0.226 nm can be easily found in PC300, which is attributed to the Pt (111) plane [30,32]. Furthermore, the element mapping images of Ce, O, and Pt in Fig. 3 show that the three elements of Ce, O, and Pt in PC400 were evenly distributed on the surface of the carbon support. The rather small loading amount of ceria explains why we cannot observe the CeO_2 diffraction peak of PC400 in the XRD patterns.

Fig. 4 exhibits the Pt 4f and Ce 3d XPS peaks for PC400, and the details of the fitting parameter results are shown in Table 1. For Pt 4f, the peaks M and M′ situated at 71.62 and 74.94 eV are ascribed to Pt^0, whereas the peaks N and N′ situated at 72.88 and 76.33 eV belong to Pt^{2+}. Pt^0 was the main Pt species in PC400, accounting for 68.1% of the total. However, compared with pure bulk Pt (70.9 eV), the binding energy showed a slight positive offset of 0.72 eV [31,36], which can be attributed to the strong interaction between Pt and CeO_2 in PC400, changing the electronic structure of the Pt metal [37–38].

With regard to Ce 3d, the U series peaks at 882.51, 885.36, 901.40, and 907.94 eV are ascribed to Ce^{3+}, whereas the six other peaks at 882.81, 888.16, 898.65, 904.15, 907.21, and 916.98 eV belong to Ce^{4+} [39]. The component proportion of Ce^{4+} was predominant, accounting for 62.2%, whereas that of Ce^{3+} was merely 37.8%. As we have previously discussed, the variable valence states (redox Ce^{3+}/Ce^{4+} sites) can greatly enhance the oxygen storage capacity, and the oxygen vacancy in Ce–O is a major advantage of the material. Yuan *et al.* [40] reported that CeO_{2-x} with a high concentration of oxygen vacancies shows good ORR activity, excellent stability, and good resistance to methanol crossover effects, thereby benefiting the catalysis of MOR.

3.2. MOR activity

Fig. 5(a) shows the CV curves of the various catalysts measured at room temperature in a 0.5 M N_2-purged H_2SO_4 solution. The ECSA values of the as-synthesized catalysts PC300, PC400, PC500, and PC600 were calculated to be 59.87, 68.14, 62.07, and 55.98 m^2·g^{-1}, which were 1.12, 1.28, 1.16, and 1.05 times higher than that of the commercial Pt/C catalyst (53.23 m^2·g^{-1}), respectively. The ECSA of each catalyst was calculated on the basis of the charges associated with the absorption peak of hydrogen after double-layer correction with a reference value of 210 μC·cm^{-2} for the hydrogen

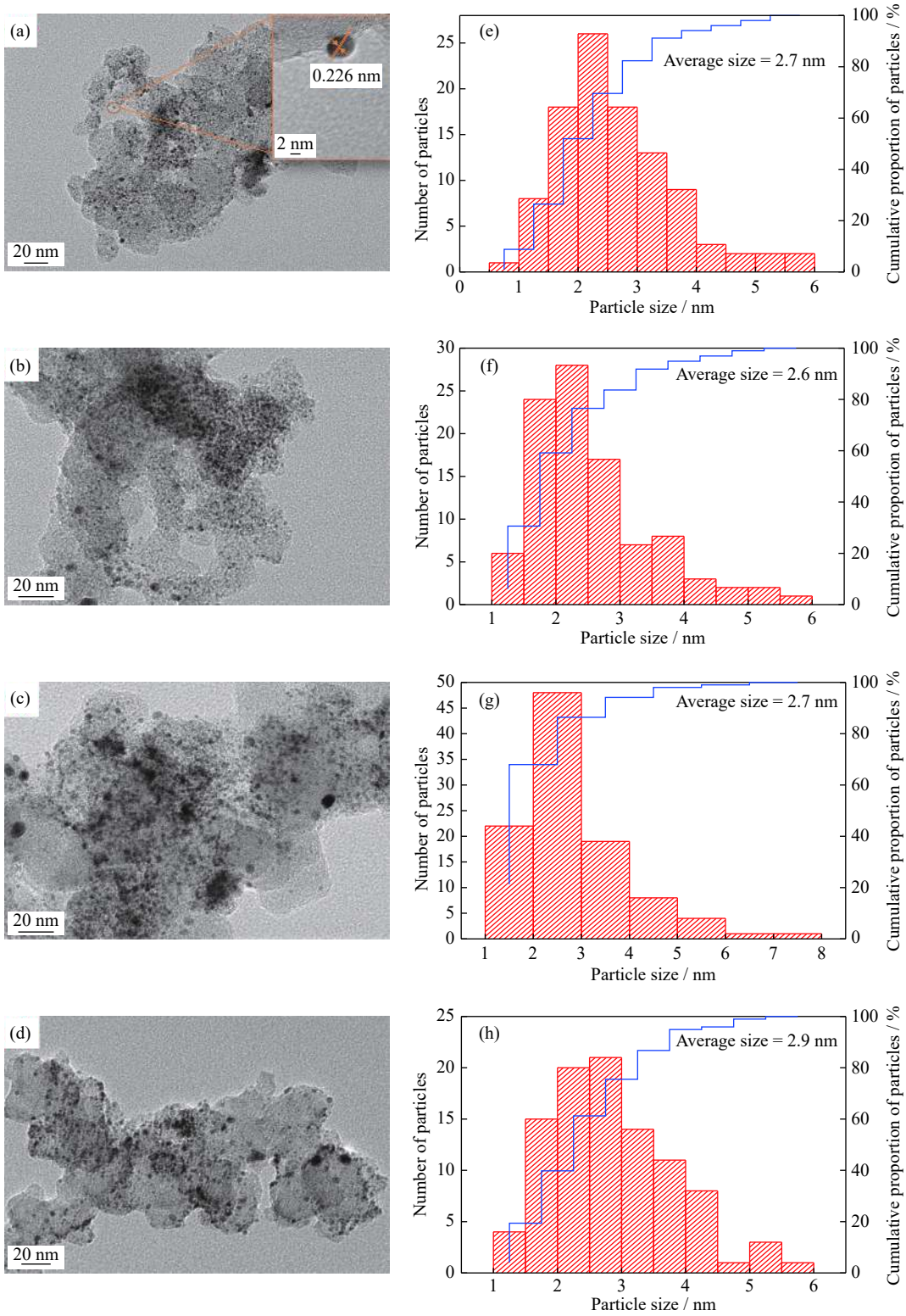

Fig. 2. (a)–(d) TEM images and (e)–(h) average particle size distribution histograms of Pt/CeO_2–C catalysts: PC300, PC400, PC500, and PC600. Inset in (a) shows the high resolution transmission electron microscope (HRTEM) images of PC300.

monolayer adsorption on the Pt surface [41]. ECSA analysis indicates that the addition of CeO_2 can facilitate electrochemical performance, and the optimal pre-calcination temperature is 400°C. The ECSA values of PC300–PC600 catalysts were larger than that of the commercial Pt/C catalyst possibly because the addition of CeO_2 can enhance the distri-

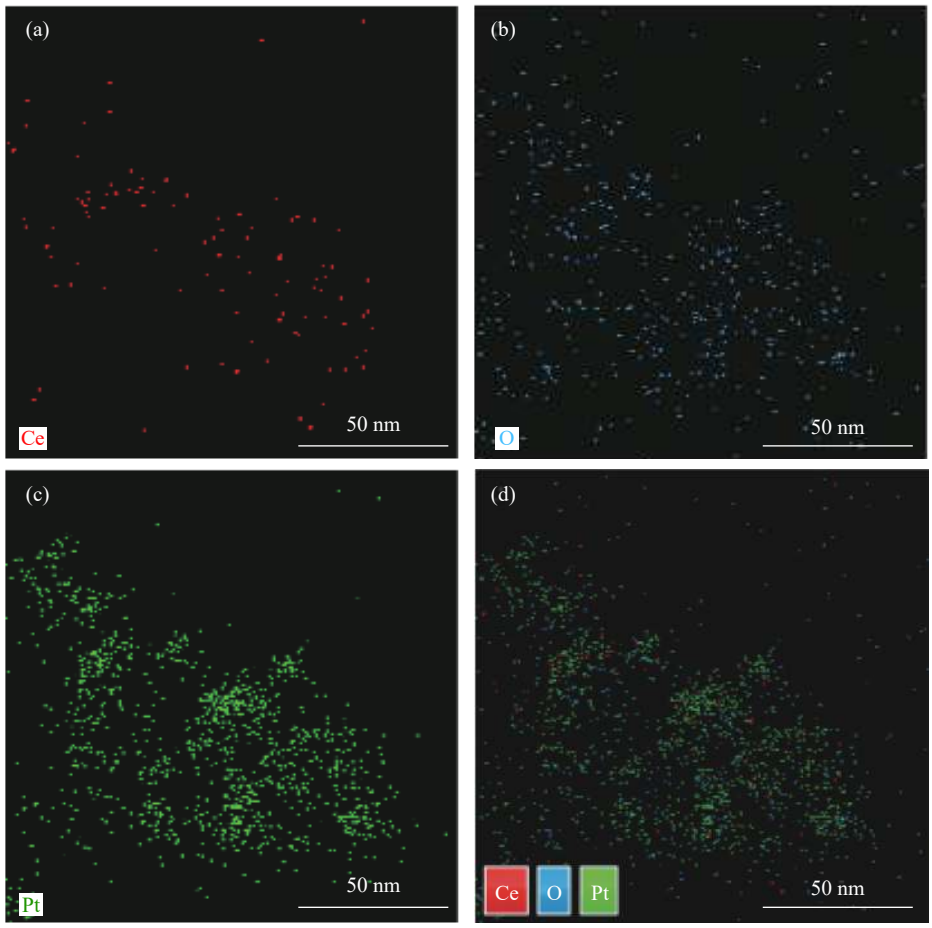

Fig. 3. TEM images of elemental mapping of (a) Ce, (b) O, (c) Pt, and (d) the overlap.

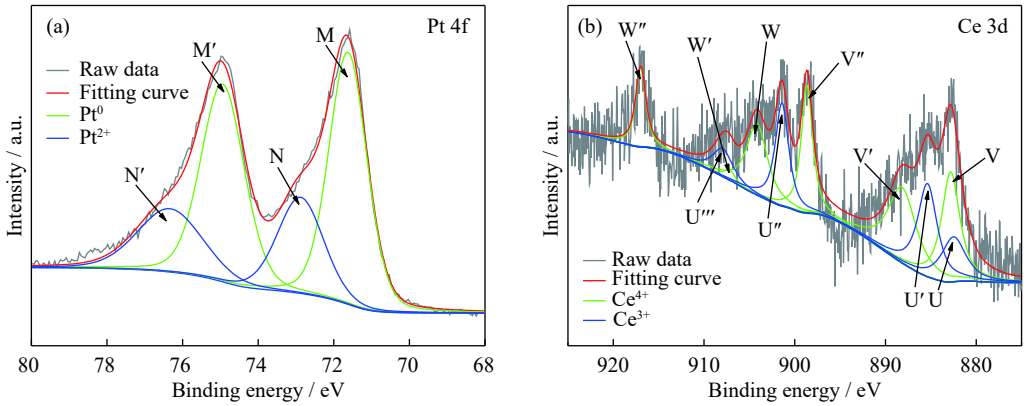

Fig. 4. XPS spectra for (a) Pt 4f and (b) Ce 3d of PC400 sample.

bution of Pt nanoparticles, which agreed with the TEM images.

Electrochemical tests of the as-prepared Pt/CeO_2–C catalysts in MOR were executed by CV measurement. As shown in Fig. 5(b) and Table 2, the onset potentials of PC300, PC600, and the commercial Pt/C started at 0.376, 0.380, and 0.383 V, respectively, which were close to each other. However, the onset potentials of PC400 and PC500 began at 0.327 and 0.33 V, respectively. A method (I_f/I_b ratio) was used to compare the ratio of the forward scanning peak current density (I_f) and the backward scanning peak current density (I_b), which represent the oxidation of methanol electro-oxidation and the subsequent oxidation of the reactive carbonaceous species obtained from the positive potential scanning, respectively [42–43]. The I_f/I_b ratio can be used to reflect the catalysts ' tolerance of CO poisoning [44]. As shown in Fig. 5(b), the I_f/I_b ratio of PC400 was the highest among all the five catalysts, including the commercial Pt/C

Table 1. Binding energies and surface compositions from deconvolution of XPS spectra in Fig. 4 for PC400

Species	Peak	Binding energy / eV	Relative proportion / %	Total proportion / %
Pt^0	M	71.62	35.90	68.1
	M′	74.94	32.20	
Pt^{2+}	N	72.88	16.50	31.9
	N′	76.33	15.40	
Ce^{4+}	V	882.81	15.42	62.2
	V′	888.16	16.45	
	V″	898.65	11.42	
	W	904.15	11.61	
	W′	907.21	0.94	
	W″	916.98	6.36	
Ce^{3+}	U	882.51	8.54	37.8
	U′	885.36	14.08	
	U″	901.40	10.81	
	U‴	907.94	4.37	

catalyst. Moreover, the I_f/I_b ratio decreased with increasing pre-calcination temperature of CeO_2 (>400°C). This result can be ascribed to the fact that the poor dispersion of the nanocatalysts directly results in poor catalytic performance and CO poisoning tolerance [45]. Compared with previous studies on Pt/CeO_2–C (graphene) systems, our results show that the CeO_2 pre-calcination temperature of the Pt/CeO_2–C catalyst affects the CO tolerance of methanol oxidation. The detailed information is provided in Table 3.

Chronoamperometry is an effective method to evaluate the electrocatalytic activity and stability of catalysts. From Fig. 6, PC400 displayed the highest current density and the smallest current decay among all the catalysts, including the commercial Pt/C. In specific, the current density values of PC300, PC400, PC500, PC600 and the commercial Pt/C after 3600 s constant potential electrolysis at 0.6 V vs. RHE in the amperometric *i–t* curves were 23.4, 28.0, 19.4, 18.1 and 12.2 $mA \cdot mg^{-1}$, respectively. This result indicates that PC400 possesses the highest electrocatalytic activity and the strongest tolerance to carbonaceous by-products produced during methanol oxidation.

The enhanced catalysis activity and stability of the as-synthesized PC300–PC600 catalysts in MOR can be explained as follows:

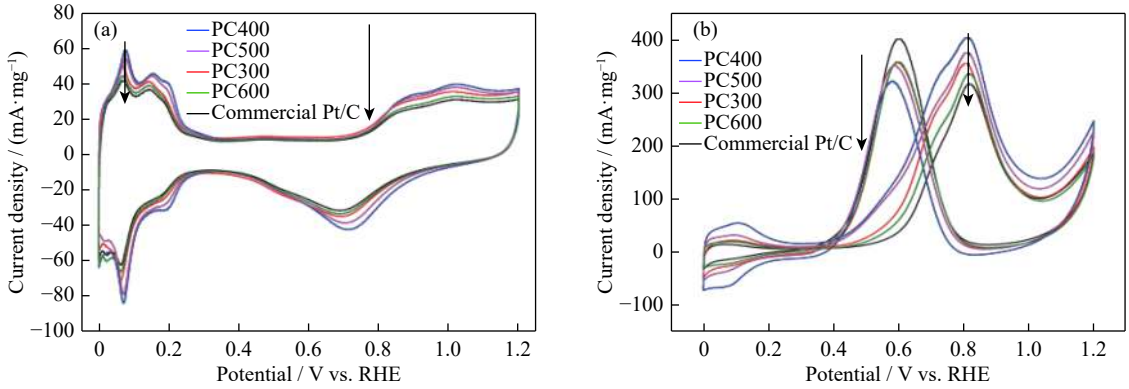

Fig. 5. Electrochemical data for the as-synthesized catalysts (PC300, PC400, PC500, and PC600) and the commercial Pt/C (20wt%, JM, America): (a) CV record in 0.5 M H_2SO_4 solution at a scan rate of 50 mV/s; (b) CV record in 1 M CH_3OH and 0.5 M H_2SO_4 solution at a scan rate of 50 mV/s.

Table 2. Comparison of electrocatalytic properties between the commercial and as-prepared catalysts

Catalyst	On-set potential / V vs. RHE	I_f / ($mA \cdot mg^{-1}$)	I_f/I_b
PC300	0.376	354	0.99
PC400	0.327	405	1.26
PC500	0.33	376	1.07
PC600	0.380	335	0.92
Commercial Pt/C	0.383	316	0.79

First, Ce 3d orbitals can change the electronic structure of Pt and weaken the adsorption of CO-based carbonaceous by-products on the Pt surface; CO can also be oxidized by CeO_2 on the Pt surface at the same time [48–49]. As a result, the reduction of carbon-containing intermediates adsorbed on the Pt surface can effectively improve the electrocatalytic activity of MOR [26].

Second, CeO_2 can improve the distribution of Pt nanoparticles [46] and provide the OH_{ad} species for electro-oxidation to interact with the carbonaceous intermediates adsorbed (CO_{ad}) by the catalysts and then generate CO_2 during MOR, which is a bi-functional mechanism. These reactions are explained as follows [50–53]:

$$CeO_2 + H_2O \rightarrow CeO_2 - OH_{ad} + H^+ + e^- \quad (2)$$

$$Pt - CO_{ad} + CeO_2 - OH_{ad} \rightarrow Pt + CeO_2 + CO_2 + H^+ + e^- \quad (3)$$

$$Pt - CeO_2 + xCO \rightarrow Pt - CeO_{2-x} + xCO_2 \quad (4)$$

Finally, the optimum pre-calcination temperature (400°C)

may contribute to the generation of CeO_2 with fluorite structure and promote the interaction among CeO_2, Pt, and carbon support. High temperatures (>400°C) may lead to the agglomeration of CeO_2, which negatively impacts the homogenous distribution of Pt nanoparticles [32,54].

Table 3. Comparison of electrocatalytic properties of I_f/I_b with previous Pt/CeO_2 studies

Catalyst	I_f/I_b	Ref.
Pt/CeO_2–graphene	<1	[46]
Pt/3wt%CeO_2–C	0.55	[47]
Pt/6wt%CeO_2–C	0.53	[47]
Pt/9wt%CeO_2–C	1.45	[47]
Pt/12wt%CeO_2–C	1.23	[47]
Pt–3wt%CeO_2/graphene	1.41	[23]
Pt–5wt%CeO_2/graphene	1.45	[23]
Pt–7wt%CeO_2/graphene	1.48	[23]
Pt–10wt%CeO_2/graphene	1.35	[23]
PC300	0.99	This work
PC400	1.26	This work
PC500	1.07	This work
PC600	0.92	This work

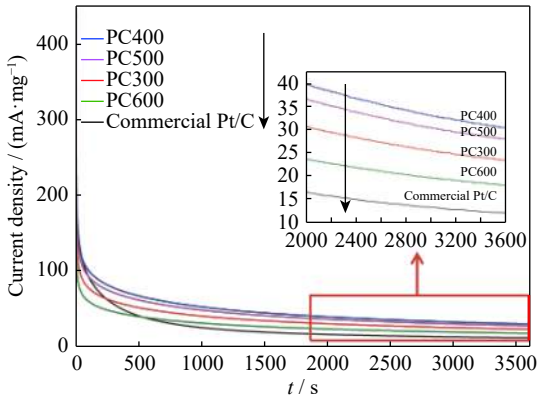

Fig. 6. Amperometric *i–t* curves collected for 1 h at 0.6 V vs. RHE for the catalysts in a 1 M CH_3OH and 0.5 M H_2SO_4 solution at room temperature.

4. Conclusion

Pt/CeO_2–C catalysts were successfully prepared, and their electrocatalytic performance was tested in acidic medium to investigate the effect of CeO_2 pre-calcined at different temperatures (300–600°C) on the performance of Pt/CeO_2–C electrocatalysts in methanol oxidation. PC400 exhibited the best methanol electro-oxidation among all the catalysts. In specific, the ECSA and I_f/I_b ratio of PC400 were 68.14 $m^2 \cdot g^{-1}$ and 1.26, respectively, which were 1.28 and 1.59 times higher than those of the commercial Pt/C catalyst. Furthermore, the amperometric *i–t* curve of PC400 displayed an excellent stability performance compared with those of the other catalysts. Therefore, introducing CeO_2 from a proper pre-calcination temperature (~400°C) can promote the dispersion of Pt nanoparticles with a small size (~2.6 nm) and provide a high tolerance to carbonaceous species produced during MOR, thereby directly enhancing catalytic activity and stability.

Acknowledgement

This work was financially supported by the National Natural Science Foundation of China (No. 51774145).

References

[1] W.X. Du, G.X. Yang, E. Wong, N.A. Deskins, A.I. Frenkel, D. Su, and X.W. Teng, Platinum–tin oxide core–shell catalysts for efficient electro-oxidation of ethanol, *J. Am. Chem. Soc.*, 136(2014), 31, p. 10862.

[2] S.S. Munjewar, S.B. Thombre, and R.K. Mallick, Approaches to overcome the barrier issues of passive direct methanol fuel cell – Review, *Renewable Sustainable Energy Rev.*, 67(2017), p. 1087.

[3] J.M. Léger, S. Rousseau, C. Coutanceau, F. Hahn, and C. Lamy, How bimetallic electrocatalysts does work for reactions involved in fuel cells?: Example of ethanol oxidation and comparison to methanol, *Electrochim. Acta*, 50(2005), No. 25-26, p. 5118.

[4] N.S. Pai, P.S. Chang, and S.K. Yen, Platinum/vivianite bifunction catalysts for DMFC, *Int. J. Hydrogen Energy*, 38(2013), No. 13, p. 5259.

[5] C. Jackson, O. Conrad, and P. Levecque, Systematic study of Pt–Ru/C catalysts prepared by chemical deposition for direct methanol fuel cells, *Electrocatalysis*, 8(2017), No. 3, p. 224.

[6] A.J. Dickinson, L.P.L. Carrette, J.A. Collins, K.A. Friedrich, and U. Stimming, Preparation of a Pt–Ru/C catalyst from carbonyl complexes for fuel cell applications, *Electrochim. Acta*, 47(2002), No. 22-23, p. 3733.

[7] V. Thiagarajan, P. Karthikeyan, R. Manoharan, S. Sampath, A. Hernández-Ramírez, M.E. Sánchez-Castro, I.L. Alonso-Lemus, and F.J. Rodríguez-Varela, Pt–Ru–$NiTiO_3$ nanoparticles dispersed on Vulcan as high performance electrocatalysts for the methanol oxidation reaction (MOR), *Electrocatalysis*, 9(2018), No. 5, p. 582.

[8] D. Pan, X.W. Li, and A.F. Zhang, Platinum assisted by carbon quantum dots for methanol electro-oxidation, *Appl. Surf. Sci.*, 427(2018), p. 715.

[9] H.S. Liu, C.J. Song, L. Zhang, J.J. Zhang, H.J. Wang, and D.P. Wilkinson, A review of anode catalysis in the direct methanol fuel cell, *J. Power Sources*, 155(2006), No. 2, p. 95.

[10] A. Glüsen, F. Dionigi, P. Paciok, M. Heggen, M. Müller, L. Gan, P. Strasser, R.E. Dunin-Borkowski, and D. Stolten, Dealloyed PtNi-core–shell nanocatalysts enable significant lowering of Pt electrode content in direct methanol fuel cells, *ACS Catal.*, 9(2019), No. 5, p. 3764.

[11] A. Serrà, M. Montiel, E. Gómez, and E. Vallés, Electrochemical synthesis of mesoporous CoPt nanowires for methanol oxidation, *Nanomaterials*, 4(2014), No. 2, p. 189.

[12] L.G. Martin, I. Green, X. Wang, S. Pasupathi, and B.G. Pollet, Pt–Sn/C as a possible methanol-tolerant cathode catalyst for DMFC, *Electrocatalysis*, 4(2013), No. 3, p. 144.

[13] S. Zhang, Z.M. Xia, T. Ni, Z.Y. Zhang, Y.Y. Ma, and Y.Q. Qu, Strong electronic metal-support interaction of Pt/CeO_2 enables efficient and selective hydrogenation of quinolines at room temperature, *J. Catal.*, 359(2018), p. 101.

[14] S.K. Meher and G.R. Rao, Polymer-assisted hydrothermal synthesis of highly reducible shuttle-shaped CeO_2: Microstructural effect on promoting Pt/C for methanol electrooxidation, *ACS Catal.*, 2(2012), No. 12, p. 2795.

[15] L. Nie, D.H. Mei, H.F. Xiong, B. Peng, Z.B. Ren, X.I.P. Hernandez, A. DeLaRiva, M. Wang, M.H. Engelhard, L. Kovarik, A.K. Datye, and Y. Wang, Activation of surface lattice oxygen in single-atom Pt/CeO_2 for low-temperature CO oxidation, *Science*, 358(2017), No. 6369, p. 1419.

[16] Z.M. Cui, L.G. Feng, C.P. Liu, and W. Xing, Pt nanoparticles supported on WO_3/C hybrid materials and their electrocatalytic activity for methanol electro-oxidation, *J. Power Sources*, 196(2011), No. 5, p. 2621.

[17] X.H. Wang, X.L. Hu, J.L. Huang, W.J. Zhang, W.J. Ji, Y. Hui, and X.X. Yao, Electrospinning synthesis of porous carbon fiber supported Pt–SnO_2 anode catalyst for direct ethanol fuel cell, *Solid State Sci.*, 94(2019), p. 64.

[18] H. Lin, Y.B. Dong, and L.Y. Jiang, Preparation of calcium carbonate particles coated with titanium dioxide, *Int. J. Miner. Metall. Mater.*, 16(2009), No. 5, p. 592.

[19] T.T. Ai, F. Wang, and X.M. Feng, Oxidation behavior of *in-situ* Al_2O_3/TiAl composites at 900°C in static air, *Int. J. Miner. Metall. Mater.*, 16(2009), No. 3, p. 339.

[20] P. Justin and G.R. Rao, Methanol oxidation on MoO_3 promoted Pt/C electrocatalyst, *Int. J. Hydrogen Energy*, 36(2011), No. 10, p. 5875.

[21] X.Y. Wang, J.C. Zhang, X.D. Cao, Y.S. Jiang, and H. Zhu, Synthesis and characterization of Pt–MoO_x–TiO_2 electrodes for direct ethanol fuel cells, *Int. J. Miner. Metall. Mater.*, 18(2011), No. 5, art. No. 594.

[22] S.Y. Song, X. Wang, and H.J. Zhang, CeO_2-encapsulated noble metal nanocatalysts: Enhanced activity and stability for catalytic application, *NPG Asia Mater.*, 7(2015), No. 5, art. No. e179.

[23] S.P. Yu, Q.B. Liu, W.S. Yang, K.F. Han, Z.M. Wang, and H. Zhu, Graphene–CeO_2 hybrid support for Pt nanoparticles as potential electrocatalyst for direct methanol fuel cells, *Electrochim. Acta*, 94(2013), p. 245.

[24] F. Xu, D.Q. Wang, B.S. Sa, Y. Yu, and S.C. Mu, One-pot synthesis of Pt/CeO_2/C catalyst for improving the ORR activity and durability of PEMFC, *Int. J. Hydrogen Energy*, 42(2017), No. 18, p. 13011.

[25] W. Wang, Y.J. Dong, Y. Yang, D. Chai, Y.M. Kang, and Z.Q. Lei, CeO_2 overlapped with nitrogen-doped carbon layer anchoring Pt nanoparticles as an efficient electrocatalyst towards oxygen reduction reaction, *Int. J. Hydrogen Energy*, 43(2018), No. 27, p. 12119.

[26] H. Xu, A.L. Wang, Y.X. Tong, and G.R. Li, Enhanced catalytic activity and stability of Pt/CeO_2/PANI hybrid hollow nanorod arrays for methanol electro-oxidation, *ACS Catal.*, 6(2016), No. 8, p. 5198.

[27] G.L. Cordeiro, E.F. de Camargo, M.C.L. Santos, C.V. Pereira, V. Ussui, N.B. de Lima, A.O. Neto, and D.R.R. Lazar, Improved Pt/CeO_2 electrocatalysts for ethanol electro-oxidation, *Int. J. Electrochem. Sci.*, 13(2018), No. 7, p. 6388.

[28] B.B. He, Q.G. Zhao, Z.G. Zeng, X.H. Wang, and S. Han, Effect of hydrothermal reaction time and calcination temperature on properties of Au@CeO_2 core–shell catalyst for CO oxidation at low temperature, *J. Mater. Sci.*, 50(2015), No. 19, p. 6339.

[29] Z.Y. Qi, C.X. Xiao, C. Liu, T.W. Goh, L. Zhou, R. Maligal-Ganesh, Y.C. Pei, X.L. Li, L.A. Curtiss, and W.Y. Huang, Sub-4 nm PtZn intermetallic nanoparticles for enhanced mass and specific activities in catalytic electrooxidation reaction, *J. Am. Chem. Soc.*, 139(2017), No. 13, p. 4762.

[30] J.J. Yang, X.Y. Tan, Y. Qian, L. Li, Y. Xue, Z. Dai, H.T. Wang, W.L. Qu, and Y.Y. Chu, Methanol oxidation on Pt/CeO_2@C–N electrocatalysts prepared by the *in-situ* carbonization of polyvinylpyrrolidone, *J. Appl. Electrochem.*, 46(2016), No. 7, p. 779.

[31] D.M. Gu, Y.Y. Chu, Z.B. Wang, Z.Z. Jiang, G.P. Yin, and Y. Liu, Methanol oxidation on Pt/CeO_2–C electrocatalyst prepared by microwave-assisted ethylene glycol process, *Appl. Catal. B*, 102(2011), No. 1-2, p. 9.

[32] J.G. Yu and B. Wang, Effect of calcination temperature on morphology and photoelectrochemical properties of anodized titanium dioxide nanotube arrays, *Appl. Catal. B*, 94(2010), No. 3-4, p. 295.

[33] F. Abbas, J. Iqbal, T. Jan, N. Badshah, Q. Mansoor, and M. Ismail, Structural, morphological, Raman, optical, magnetic, and antibacterial characteristics of CeO_2 nanostructures, *Int. J. Miner. Metall. Mater.*, 23(2016), No. 1, p. 102.

[34] Z.Y. Cai, B. Song, L.F. Li, Z. Liu, and X.K. Cui, Effect of CeO_2 on heat transfer and crystallization behavior of rare earth alloy steel mold fluxes, *Int. J. Miner. Metall. Mater.*, 26(2019), No. 5, p. 565.

[35] K. Fugane, T. Mori, D.R. Ou, A. Suzuki, H. Yoshikawa, T. Masuda, K. Uosaki, Y. Yamashita, S. Ueda, K. Kobayashi, N. Okazaki, I. Matolinova, and V. Matolin, Activity of oxygen reduction reaction on small amount of amorphous CeO_x promoted Pt cathode for fuel cell application, *Electrochim. Acta*, 56(2011), No. 11, p. 3874.

[36] B.J. Kennedy and A. Hamnett, Oxide formation and reactivity for methanol oxidation on platinised carbon anodes, *J. Electroanal. Chem. Interfacial Electrochem.*, 283(1990), No. 1-2, p. 271.

[37] F. Larachi, J. Pierre, A. Adnot, and A. Bernis, Ce 3d XPS study of composite $Ce_xMn_{1-x}O_{2-y}$ wet oxidation catalysts, *Appl. Surf. Sci.*, 195(2002), No. 1-4, p. 236.

[38] J. Zhao, W.X. Chen, Y.F. Zheng, and X. Li, Novel carbon supported hollow Pt nanospheres for methanol electrooxidation, *J. Power Sources*, 162(2006), No. 1, p. 168.

[39] A.B. Yousaf, M. Imran, N. Uwitonze, A. Zeb, S.J. Zaidi, T.M. Ansari, G. Yasmeen, and S. Manzoor, Enhanced electrocatalytic performance of Pt_3Pd_1 alloys supported on CeO_2/C for methanol oxidation and oxygen reduction reactions, *J. Phys. Chem. C*, 121(2017), No. 4, p. 2069.

[40] X.T. Yuan, H.X. Ge, X.Y. Liu, X. Wang, W.G. Chen, W.J. Dong, and F.Q. Huang, Efficient catalyst of defective CeO_{2-x} and few-layer carbon hybrid for oxygen reduction reaction, *J. Alloys Compd.*, 688(2016), p. 613.

[41] C. Wei, S.N. Sun, D. Mandler, X. Wang, S.Z. Qiao, and Z.J. Xu, Approaches for measuring the surface areas of metal oxide electrocatalysts for determining their intrinsic electrocatalytic activity, *Chem. Soc. Rev.*, 48(2019), No. 9, p. 2518.

[42] Y.C. Zhao, L. Zhan, J.N. Tian, S.L. Nie, and Z. Ning, Enhanced electrocatalytic oxidation of methanol on Pd/polypyrrole–graphene in alkaline medium, *Electrochim. Acta*, 56(2011), No. 5, p. 1967.

[43] C.C. Ting, C.H. Chao, C.Y. Tsai, I.K. Cheng, and F.M. Pan, Electrocatalytic performance of Pt nanoparticles sputter-deposited on indium tin oxide toward methanol oxidation reaction: The particle size effect, *Appl. Surf. Sci.*, 416(2017), p. 365.

[44] F.W. Zhan, T. Bian, W.G. Zhao, H. Zhang, M.S. Jin, and D.R. Yang, Facile synthesis of Pd–Pt alloy concave nanocubes with high-index facets as electrocatalysts for methanol oxidation, *CrystEngComm*, 16(2014), No. 12, p. 2411.

[45] G.L. Bai, C. Liu, Z. Gao, B.Y. Lu, X.L. Tong, X.Y. Guo, and N.J. Yang, Atomic carbon layers supported Pt nanoparticles for minimized CO poisoning and maximized methanol oxidation, *Small*, 15(2019), No. 38, art. No. 1902951.

[46] H.L. Chen, J.L. Duan, X.L. Zhang, Y.F. Zhang, C. Guo, L. Nie, and X.W. Liu, One step synthesis of Pt/CeO_2–graphene catalyst by microwave-assisted ethylene glycol process for direct methanol fuel cell, *Mater. Lett.*, 126(2014), p. 9.

[47] M.A. Scibioh, S.K. Kim, E.A. Cho, T.H. Lim, S.A. Hong, and H.Y. Ha, Pt–CeO_2/C anode catalyst for direct methanol fuel cells, *Appl. Catal. B*, 84(2008), No. 3-4, p. 773.

[48] C.T. Campbell and C.H.F. Peden, Oxygen vacancies and catalysis on ceria surfaces, *Science*, 309(2005), No. 5735, p. 713.

[49] E. Mamontov, W. Dmowski, T. Egami, and C.C. Kao, Electronic excitation in a catalytic support oxide, CeO_2, *J. Phys. Chem. Solids*, 61(2000), No. 3, p. 431.

[50] K. Yoon, Y. Yang, P. Lu, D.H. Wan, H.C. Peng, K.S. Masias, P.T. Fanson, C.T. Campbell, and Y.N. Xia, A highly reactive and sinter-resistant catalytic system based on platinum nanoparticles embedded in the inner surfaces of CeO_2 hollow fibers, *Angew. Chem. Int. Ed.*, 51(2012), No. 38, p. 9543.

[51] A. Kabbabi, R. Faure, R. Durand, B. Beden, F. Hahn, J.M. Leger, and C. Lamy, *In situ* FTIRS study of the electrocatalytic oxidation of carbon monoxide and methanol at platinum–ruthenium bulk alloy electrodes, *J. Electroanal. Chem.*, 444(1998), No. 1, p. 41.

[52] M.-S. Ekrami-Kakhki, N. Farzaneh, S. Abbasi, and B. Makiabadi, Electrocatalytic activity of Pt nanoparticles supported on novel functionalized reduced graphene oxide–chitosan for methanol electrooxidation, *J. Mater. Sci.: Mater. Electron.*, 28(2017), No. 17, p. 12373.

[53] S. Ramani, S. Sarkar, V. Vemuri, and S.C. Peter, Chemically designed CeO_2 nanoboxes boost the catalytic activity of Pt nanoparticles toward electro-oxidation of formic acid, *J. Mater. Chem. A*, 5(2017), No. 23, p. 11572.

[54] J.J. Yang, Y.Y. Chu, L. Li, H.T. Wang, Z. Dai, and X.Y. Tan, Effects of calcination temperature and CeO_2 contents on the performance of Pt/CeO_2−CNTs hybrid nanotube catalysts for methanol oxidation, *J. Appl. Electrochem.*, 46(2016), No. 3, p. 369.